SERDP

INTERIM REPORT

Applications of the Coupled-Finite/Boundary Element (CFEBE) Technique to Support the Support UXO Remediation Systems

Ahmad Abawi
HLS Research

December 2023

SERDP Project MR21-1275

REPORT DOCUMENTATION PAGE

Form Approved
OMB No. 0704-0188

1. REPORT DATE *(DD-MM-YYYY)*	**2. REPORT TYPE**	**3. DATES COVERED** *(From - To)*
31/12/2023	SERDP Interim Report	12/7/2021 - 1/31/2025

4. TITLE AND SUBTITLE

Applications of the Coupled-Finite/Boundary Element (CFEBE) Technique to Support the Support UXO Remediation Systems

5a. CONTRACT NUMBER
22-C-0012

5b. GRANT NUMBER

5c. PROGRAM ELEMENT NUMBER

6. AUTHOR(S)
Ahmad Abawi

5d. PROJECT NUMBER
MR21-1275

5e. TASK NUMBER

5f. WORK UNIT NUMBER

7. PERFORMING ORGANIZATION NAME(S) AND ADDRESS(ES)
HLS Research
12625 High Bluff Drive, Suite 211
San Diego, CA 92130

8. PERFORMING ORGANIZATION REPORT NUMBER
MR21-1275

9. SPONSORING/MONITORING AGENCY NAME(S) AND ADDRESS(ES)
Office of the Deputy Assistant Secretary of Defense (Energy Resilience & Optimization)
3500 Defense Pentagon, RM 5C646
Washington, DC 20301-3500

10. SPONSOR/MONITOR'S ACRONYM(S)
SERDP

11. SPONSOR/MONITOR'S REPORT NUMBER(S)
MR21-1275

12. DISTRIBUTION/AVAILABILITY STATEMENT
DISTRIBUTION STATEMENT A. Approved for public release: distribution unlimited.

13. SUPPLEMENTARY NOTES

14. ABSTRACT
The objective of this project is to compute the bistatic scattering amplitudes for UXO targets for use in the TIER model to simulate an experimental scenario for detection, localization and identification of these targets. The mathematical details and the rationale for the geometries used in computing the bistatic scattering amplitudes were presented within this interim report.

15. SUBJECT TERMS
Coupled-Finite, Boundary Element Technique, CFEBE, UXO, Remediation Systems

16. SECURITY CLASSIFICATION OF:			**17. LIMITATION OF ABSTRACT**	**18. NUMBER OF PAGES**	**19a. NAME OF RESPONSIBLE PERSON**
a. REPORT	**b. ABSTRACT**	**c. THIS PAGE**			Ahmad Abawi
UNCLASS	UNCLASS	UNCLASS	UNCLASS	19	**19b. TELEPHONE NUMBER** *(Include area code)* 858-336-6409

Interim Report 2

Contents

1 Objective **1**

2 Background and technical approach **1**

3 Results and discussion **3**
3.1 Target *c* 5
3.2 Target *b* 9
3.3 Target *d* 11
3.4 Target *e* 12

4 Summary and conclusions **14**

List of Figures

1 *The scattered field due to the presence of the interface is approximated by the contribution of four principal ray paths in the TIER model. The arrows indicate how the incident ray is scattered by the target and the interface.* 2
2 *The geometry of scattering from the target, the image target, and the interface. S/R represents the location of source and receiver, which are collocated.* 2
3 *Distribution of points on the surface of a sphere of 10-m radius using the Golden Spiral method on the left and on latitudes and longitudes on the right. The Golden Spiral method produces a more evenly distribution of points.* 3
4 *Pictures and CAD drawings of some of the UXOs used for current and future modeling.* 4
5 *Material properties for targets b − e. Note that the targets are not to scale with respect to each other.* 4
6 *The coordinate planes where the axis of the target coincides with z-axis.* 5

7 *Panels (a) and (b) show the acoustic color, computed directly, in xz and the xy planes with the target's axis along the z-axis (see Fig. (6)). Panel (c) shows that the acoustic color in the xz plane almost identically reconstructed from the bistatic scattering amplitudes computed at points on the surface of a sphere of 10-m radius shown in Fig. (3a).* 6
8 *The source and the receiver triangles used for interpolation.* 7
9 *Projections of the scattered field onto the coordinate surfaces. The direction of the incident field is shown in the far right of the figure. Each row shows the results for the indicated incident field and contains the scattered field in the three coordinate planes defined in Fig. (6). The xz plane is the plane of the paper.* 9
10 *Panels (a) and (b) show the acoustic color, computed directly, in xz and the xy planes with the target's axis along the z-axis. Panel (c) shows that the acoustic color in the xz plane reconstructed from the bistatic scattering amplitudes computed at points on the surface of a sphere of 10-m radius.* 10
11 *Projections of the scattered field onto the coordinate surfaces for the 155mm M107 Howitzer. The direction of the incident field is shown in the far right of the figure. Each row shows the results for the indicated incident field and contains the scattered field in the three coordinate planes defined in Fig. (6). The xz plane is the plane of the paper.* 10
12 *Panels (a) and (b) show the acoustic color, computed directly, in xz and the xy planes with the target's axis along the z-axis. Panel (c) shows that the acoustic color in the xz plane reconstructed from the bistatic scattering amplitudes computed at points on the surface of a sphere of 10-m radius.* 11
13 *Projections of the scattered field onto the coordinate surfaces for the 105mm M60. The direction of the incident field is shown in the far right of the figure. Each row shows the results for the indicated incident field and contains the scattered field in the three coordinate planes defined in Fig. (6). The xz plane is the plane of the paper.* 12
14 *Panels (a) and (b) show the acoustic color, computed directly, in xz and the xy planes with the target's axis along the z-axis. Panel (c) shows that the acoustic color in the xz plane reconstructed from the bistatic scattering amplitudes computed at points on the surface of a sphere of 10-m radius.* 13
15 *Projections of the scattered field onto the coordinate surfaces for the 81mm mortar shell. The direction of the incident field is shown in the far right of the figure. Each row shows the results for the indicated incident field and contains the scattered field in the three coordinate planes defined in Fig. (6). The xz plane is the plane of the paper.* 13

Abstract

Progress during the second year of this project is summarized in this report. It briefly describes the method of and the rationale for the computation of bistatic scattering amplitudes on the surface of a sphere of 10-m radius. Methods were developed to reproduce known results, such as the acoustic color from the bistatic scattering data to not only validate the methods used to produce them, but also gain physical insight into the nature of the scattering problem. These methods include an interpolation technique for reconstructing the acoustic color from the bistatic scattering data and back propagation of the data from the surface of the 10-m sphere onto the coordinate surfaces. These techniques are applied to four targets and the results are presented and analyzed.

1 Objective

The objective of this project is to compute the bistatic scattering amplitudes for UXO targets for use in the TIER model to simulate an experimental scenario for detection, localization and identification of these targets. The mathematical details and the rationale for the geometries used in computing the bistatic scattering amplitudes were presented in our first interim report submitted on Dec/31/2022. In this report we briefly mention them for completeness.

2 Background and technical approach

Scattering from complex, UXO-like targets is computed using the Coupled Finite Element /Boundary Element method or CFEBE [1]. In this model, the finite element technique is used to compute the free modes of vibration of the target in vacuum, which provides the complete solution for the response of the target to any type of mechanical excitation. When the target is immersed in a fluid environment with a known Green's function, the effects of the fluid loading and the incident field are incorporated into the solution by the application of the boundary conditions using the boundary element method.

Even though the CFEBE model is capable of computing scattering from an arbitrary target in an arbitrary ocean environment, under this project it is primarily used to compute scattering from targets in free space as input to the TIER model, through which environmental effects are added by an approximate method. However, since the CFEBE model can self-consistently include the effects of the environment by using the appropriate Green's function, it can also be used to validate the TIER solution.

According to the TIER model, the scattered pressure in the presence of an interface (environment) can be approximated by four ray paths associated with the actual source and receiver and their images in the sediment [2]. This is true based on two conditions: 1) the air–water interface can be ignored, because paths that interact with this interface are either removed by time gating the received signals or suppressed by the directivity patterns of the source and the receiver and 2) the distance between the actual source and the actual receiver is much smaller than the distance between source to target and target to receiver. The latter condition allows the assumption that the source and receiver are co-located. The four principal ray paths contributing to the scattered field are shown in Fig. (1).

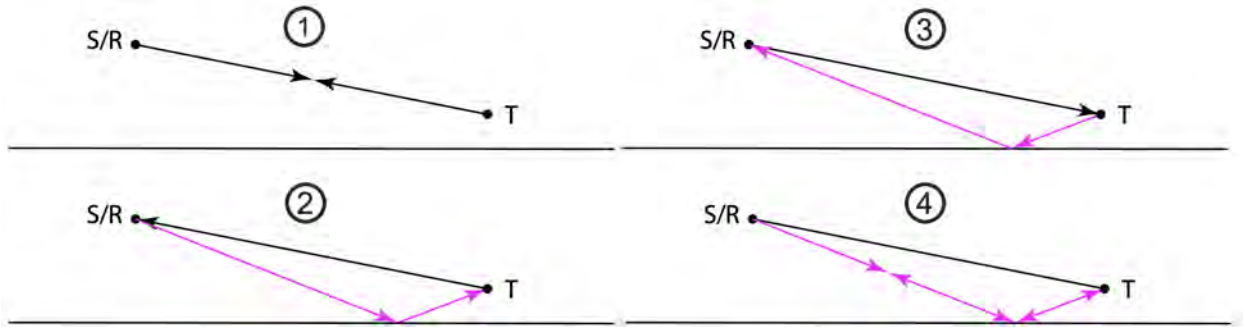

Figure 1: *The scattered field due to the presence of the interface is approximated by the contribution of four principal ray paths in the TIER model. The arrows indicate how the incident ray is scattered by the target and the interface.*

Referring to Fig. (2),

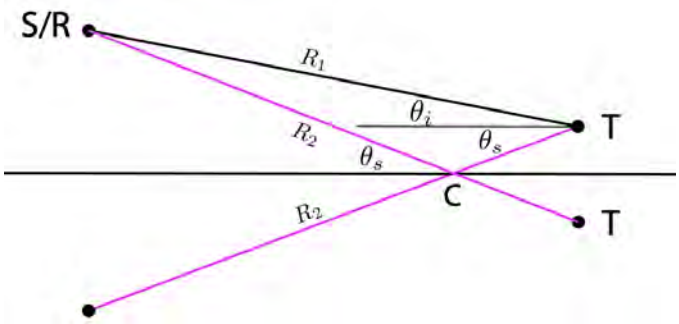

Figure 2: *The geometry of scattering from the target, the image target, and the interface. S/R represents the location of source and receiver, which are collocated.*

the acoustic field is given by

$$P_{scat}(\theta_i,\theta_s) = P(\theta_i,\theta_i)\frac{e^{2ikR_1}}{R_1^2} + 2R(\theta_s)P(\theta_i,\theta_s)\frac{e^{ik(R_1+R_2)}}{R_1R_2} + R^2(\theta_s)P(\theta_s,\theta_s)\frac{e^{2ikR_2}}{R_2^2}, \tag{1}$$

where R_1 is the distance between the source to the target, R_2 is the distance from the source to the image target and $R(\theta)$ is plane wave reflection coefficient for the interface. $P(\theta_1,\theta_2)$ is the bistatic scattering amplitude for an incident angle θ_1 and scattering angle θ_2. Equation (1) is the TIER approximation for the pressure field scattered from a target at angle θ_s due to an incident plane wave at angle θ_i. The TIER model accounts for the presence of the interface by two monostatic and two bistatic free space scattering amplitudes, $P(\theta_1,\theta_2)$, multiplied by the appropriate phases. To use this formulation to compute the target strength for a general target for arbitrary source and receiver angles, the free space, bistatic scattering amplitudes, P, must be computed for all frequencies of interest at a large number of source and receiver angles. This is the primary task of this project.

The bistatic scattering amplitudes are computed for N source and N receiver locations on the surface of a sphere of 10-m radius for M frequencies [1]. This results in a large amount of data, i.e.,

[1]The reason this radius is chosen is to eliminate near-field effects since TIER is a far-field model.

($N \times N \times M$), which can easily exceed may hundreds of gigabytes (GBs). For this reason, care must be exercised to determine the most efficient way the points are distributed on the surface of the sphere. In this case 'efficient' implies the smallest number of points that can adequately sample the acoustic field.

In our 2022 Interim Report we used the Golden Spiral rule [3], suggested by Steve Kargl of APL-UW, as an efficient way of distributing the source/receiver points on the surface of the sphere. The left panel in Fig. (3) shows the distribution of points on the surface of a sphere of 10-m radius using the Golden Spiral method and the right panel shows almost the same number of points distributed on latitudes and longitudes with an angular separation of 4°. Note that in the latter case 90 points are distributed around each latitude regardless of the length of its circumference. This results in the proliferation of points as one approaches the poles.

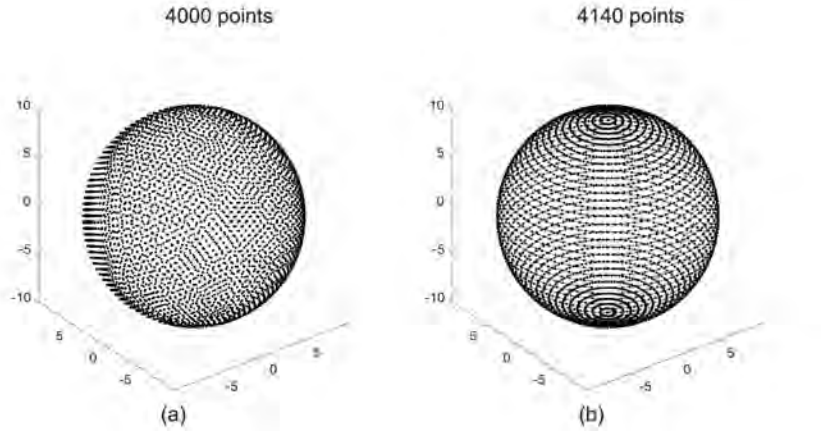

Figure 3: *Distribution of points on the surface of a sphere of 10-m radius using the Golden Spiral method on the left and on latitudes and longitudes on the right. The Golden Spiral method produces a more evenly distribution of points.*

Once the question of point distribution was settled, we gave mathematical reasoning for the minimum required number of points on the surface of the sphere needed to adequately sample the acoustic field. Based on this analysis, which was reported in our 2022 Interim Report, we showed that the minimum required number of points on the surface of a sphere of 10-m radius should be around 4000 for a maximum frequency of 30 kHz. This number is consistent with the results of a simulation study by Steve Kargl of APL-UW [4], where he studied the convergence of a broadband field scattered by a 1 × 2-foot rigid finite cylinder as a function of the number of points on the surface of the sphere where the bistatic scattering amplitudes were computed.

3 Results and discussion

An updated set of pictures and CAD drawings of the targets for which we have computed the bistatic scattering amplitudes is shown Figure (4)

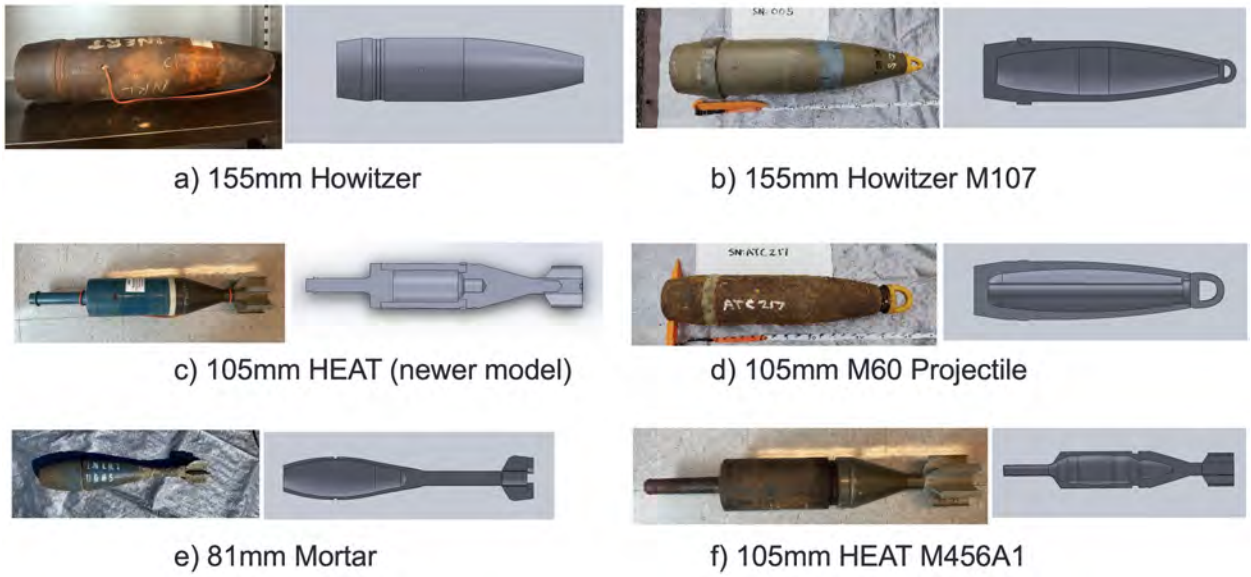

Figure 4: *Pictures and CAD drawings of some of the UXOs used for current and future modeling.*

This is a sample of a larger collection of targets that will be modeled. In this report, we will show results for targets $b - e$, where the results for targets c and e, which were included in our 2022 Interim Report have been updated. We are currently working on target f. Note that CAD data must not only contain an accurate geometry of the target, but also its material properties. Obtaining a thorough knowledge of both has turned out to be quite challenging, and in some cases like those for targets c and e they needed to be revised. The material properties for targets $b - e$ are listed in Fig. (5)

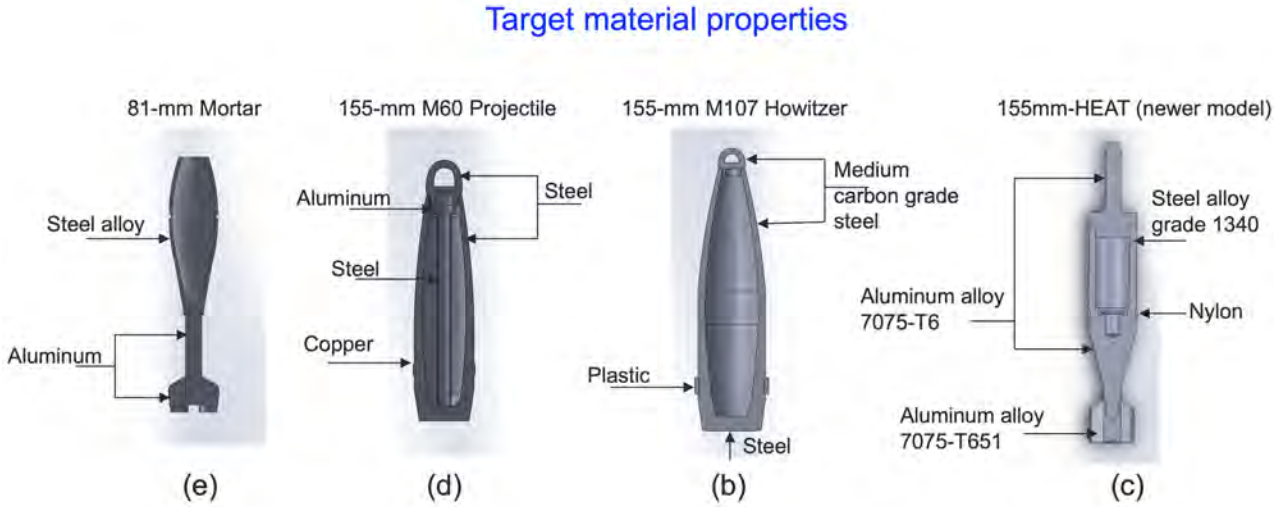

Figure 5: *Material properties for targets $b - e$. Note that the targets are not to scale with respect to each other.*

The process of generating the bistatic scattering amplitudes on the surface of 10-m sphere starts with obtaining the target CAD file from APL-UW. The CAD file is used to mesh the target and assign material properties to its different parts. The mesh is then fed into another finite element model that computes the target vibrational modes, which are finally fed into the CFEBE [1] model to compute the bistatic scattering amplitudes. However, before computing the more numerically-intensive bistatic scattering amplitudes, we compute the acoustic color for each target to make sure the model works properly. In some cases, we also compute the target mode shapes and its resonant frequencies as another sanity check.

Unlike the acoustic color, the bistatic data is quite abstract and does not easily lend itself to physical intuition. For this reason, during this year, we have adopted other means of checking the correctness and accuracy of the generated data. One is to compute the acoustic color from the bistatic data by a more sophisticated interpolation technique. The other is to investigate the data in the time domain by projecting the field from the surface of the 10-m sphere onto the coordinate planes where the target is located. These methods will be discussed when we present the results for the first target in the next section and similar results will be presented for the other targets in the following sections.

3.1 Target *c*

All four targets that will be discussed in this report are non-axially symmetric. For these targets the acoustic color assumes a broader description, as it can be computed in the xy plane, which is perpendicular to the axis of the target as well as any plane containing the axis of the target, including the xz plane. Obviously, for an axially symmetric target the acoustic color in the xy plane is constant for all angles at a given frequency and it is the same for any plane containing the axis of the target. For this reason, a single acoustic color plot in any plane containing the axis of symmetry of an axially symmetric target is "the acoustic color plot" for that target.

The results for target *c* are shown in Fig. (7), where the CAD representations of the exterior and interior of the target are shown in the far left and far right of the figure, respectively. To explain the results in the middle three panels of Fig. (7), consider the coordinate planes in Fig. (6) where the axis of the target (not shown) coincides with the z-axis

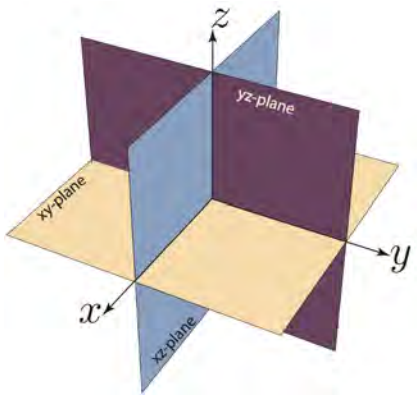

Figure 6: *The coordinate planes where the axis of the target coincides with z-axis.*

Figure (7a) shows the acoustic color in the xz plane, where the collocated source and receiver (S/R)

sweeps the polar angle, θ, in the xz plane from zero to 180°. Figure (7b) shows the acoustic color in the xy plane, where the S/R sweeps the azimuthal angle ϕ in the xy plane from zero to 360°. The results in Figs. (7a) and (7b) have been computed directly, where the former is the familiar acoustic color. If the target were axially symmetric, the results in Fig. (7b) would have been constant for all angles, as is the case here for frequencies less than 10 kHz.

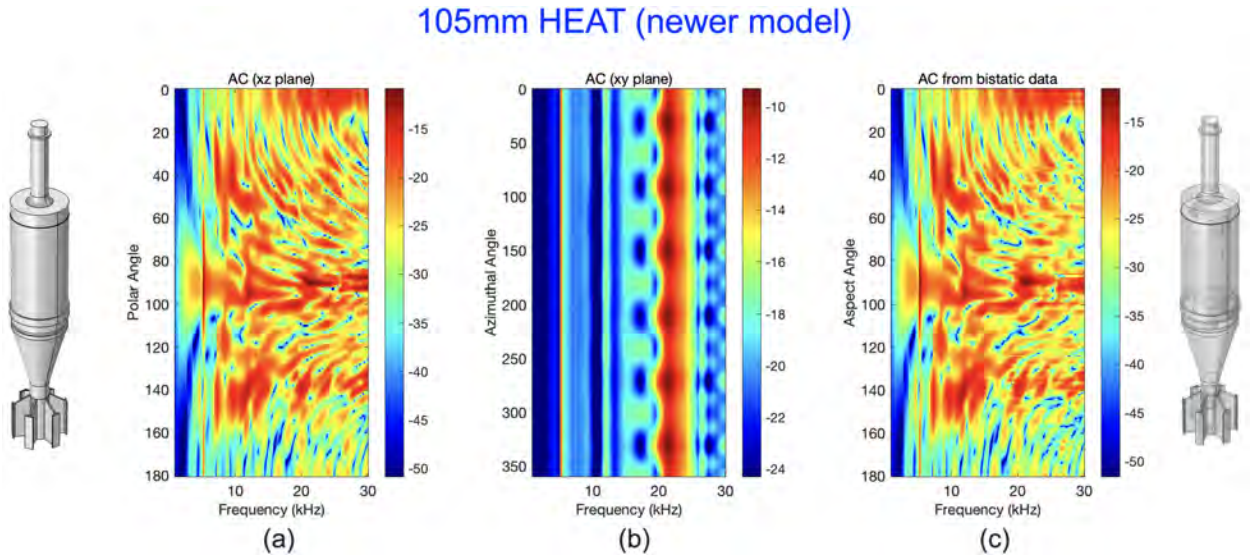

Figure 7: *Panels (a) and (b) show the acoustic color, computed directly, in xz and the xy planes with the target's axis along the z-axis (see Fig. (6)). Panel (c) shows that the acoustic color in the xz plane almost identically reconstructed from the bistatic scattering amplitudes computed at points on the surface of a sphere of 10-m radius shown in Fig. (3a).*

However, for frequencies larger than 10 kHz, Fig. (7b) shows some interesting features. At around 17 kHz scattering from the fins can be seen as S/R goes around the target. The alternating bright and dark patterns show in-phase and out-of-phase scattering from the fins and the gap between them. At higher frequencies scattering from the edges of the fins as well as from the edges formed by the intersection of the fins with the body of the target can be seen.

Figure (7c) is a reconstruction of Fig. (7a) from the bistatic data. Note that the bistatic data are stored at 4000 source and 4000 receiver points. To extract the pressure value, both the source and the receiver indices, as well as the frequency index must be specified. To obtain the pressure value for an arbitrary source and receiver location, one would have to use interpolation. For this purpose, let us define the distance matrix for the source and the receiver,

$$\begin{aligned} D_s &= \sqrt{((x_s - X_s)^2 + (y_s - Y_s)^2 + (z_s - Z_s)^2)}, \\ D_r &= \sqrt{((x_r - X_r)^2 + (y_r - Y_r)^2 + (z_r - Z_r)^2)}, \end{aligned} \tag{2}$$

where (x_s, y_s, z_s) and (x_r, y_r, z_r) are the locations of the source and the receiver where the value of pressure, $P(\vec{r}_s, \vec{r}_r)$, is desired, $\vec{R}_s = (X_s, Y_s, Z_s)$ and $\vec{R}_r = (X_r, Y_r, Z_r)$ are the locations of the source and receiver on the surface of the 10-m sphere where the pressure, $\tilde{P}(\vec{R}_s, \vec{R}_r)$ is stored. In the above (x_s, y_s, z_s) are the components of $\vec{r}_s$, (x_r, y_r, z_r) are the components of $\vec{r}_r$ and so on. The

simplest way that $P(\vec{r}_s, \vec{r}_r)$ can be obtained by interpolation is to select the value of $\tilde{P}(\vec{R}_s, \vec{R}_r)$ that is nearest neighbor to $(\vec{r}_s, \vec{r}_r)$. In other words, that value of $\tilde{P}$ for which D_s and D_r are minimum. We applied this technique to reconstruct the acoustic color from bistatic data for the 105mm HEAT Practice Round in our 2022 Interim Report (see Fig. (10)), but the results were not satisfactory since this is the lowest order interpolation.

This year we developed a more rigorous and accurate interpolation method by using the distance matrices in (2) to not just get the closest points to $(\vec{r}_s, \vec{r}_r)$, but three nearest neighbors to it. To explain this, we use the triangles shown in Fig. (8).

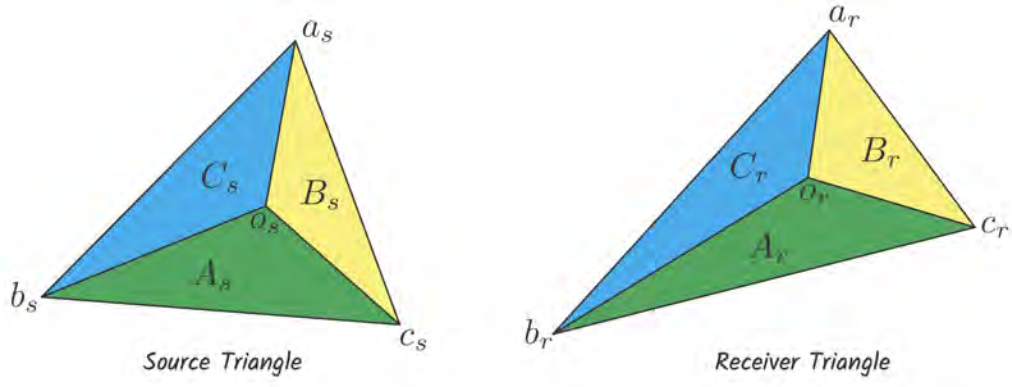

Figure 8: *The source and the receiver triangles used for interpolation.*

If the pressure values, $P(a_s)$, $P(b_s)$ and $P(c_s)$, were known at the vertices (a_s, b_s, c_s) of say the triangle on the left, then it is well known that its average value at point O_s would be

$$P(O_s) = \frac{P(a_s)A_s + P(b_s)B_s + P(c_s)C_s}{(A_s + B_s + C_s)},$$

where A_s, B_s and C_s are the areas of the three sub-triangles. However, in our case the pressure value cannot be determined unless the receiver points have also been specified, which necessitates the use of the triangle on the right. This presents many choices of different combinations of source and receiver points, which we have tried and found that they all result in about the same pressure estimates. The combination that we used gets the first estimate of the pressure by using the source triangle,

$$P_1(O_s) = \frac{P(a_s, a_r)A_s + P(b_s, b_r)B_s + P(c_s, c_r)C_s}{(A_s + B_s + C_s)}, \tag{3}$$

and another estimate using the receiver triangle,

$$P_2(O_r) = \frac{P(a_s, a_r)A_r + P(b_s, b_r)B_r + P(c_s, c_r)C_r}{(A_r + B_r + C_r)}, \tag{4}$$

from which a final estimate can be obtained by averaging the two quantities

$$P(O_s, O_r) = \frac{P_1(O_s) + P_2(O_r)}{2}. \tag{5}$$

Note that it is perfectly reasonable to use any combinations of $P(a_s, c_r)$, $P(c_s, b_r)$ and so on, but as was stated, this makes little difference in the estimate of $P(O_s, O_r)$.

The results in Fig. (7c) were computed using the bistatic scattering amplitudes on the surface of a sphere of 10-m radius and the technique described by (3 – 5). As can be seen, it reproduces the acoustic color computed directly in Fig. (7a) almost exactly. This is a solid confirmation that the bistatic scattering amplitudes computed on the surface of the 10-m sphere are consistent with the direct computation of the acoustic color. It is also a further verification of the choice of the number and distribution of source/receiver points on the surface of the sphere.

Another way to examine the bistatic amplitudes data and learn more about how the acoustic field is scattered by the target is to fix the direction of the incident field and project the acoustic field from all points on the surface of the 10-m sphere to points on the coordinate planes shown in Fig. (6). We then Fourier transformed the projected field to the time domain and plotted the bin that contained the peak signal. This is equivalent to back propagating the maximum scattered signal from each point on the surface of the sphere to every point on the coordinate surfaces.

The results for Target *c* are shown in Fig. (9), where each row is for a different incident field the direction of which is indicated by the arrow in the far right of the figure. The top left panel shows the field scattered from the target in the xy plane. Since the field in this case incident along the axis of the target, we see it is scattered uniformly in the xy plane. The middle and the right panels in the top row look almost identical, consistent with the results in the top left panel, showing that for this incident field the scattering is uniform in the azimuthal direction, despite the presence of the fins, which have a very small cross section for this direction of the incident field.

The results in the bottom row are much more interesting, where each panel has a unique scattering signature. The bottom left panel shows that the circular part of the target is mostly responsible for scattering in this plane for an incident field that parallel to it. The bottom middle and right panels do show the effects of scattering from the fins. The scattered field in the bottom right panel is symmetric with respect to the axis of the target. The reason for this is that the yz plane is perpendicular to the plane of the paper on which the target is symmetric with respect to its axis, both sides of which are exposed to the same incident field.

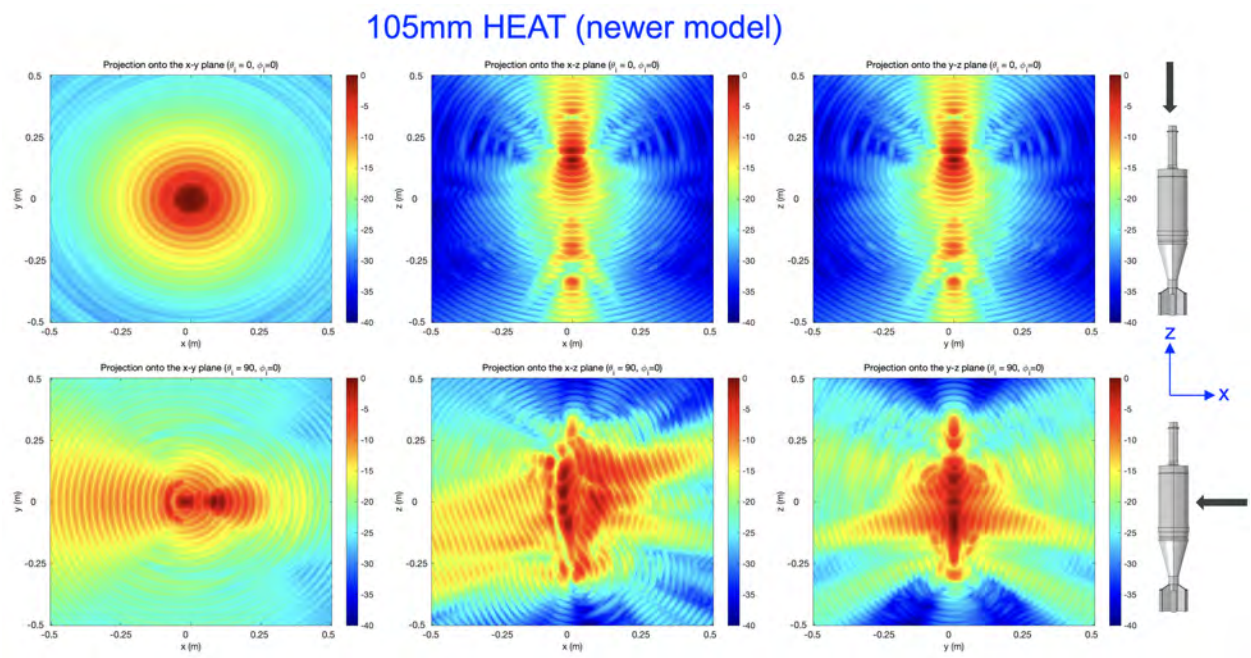

Figure 9: *Projections of the scattered field onto the coordinate surfaces. The direction of the incident field is shown in the far right of the figure. Each row shows the results for the indicated incident field and contains the scattered field in the three coordinate planes defined in Fig. (6). The xz plane is the plane of the paper.*

The interpolation method described by (3 – 5) not only validates the computation and the spatial distribution of the bistatic scattering amplitudes, but it also proves that it can be used as an accurate and robust method for use in TIER, i.e., in (1) where this type of interpolation is needed.

In the next three sections we will present similar results for the other three targets.

3.2 Target *b*

This target is the 155mm M107 Howitzer. Bistatic scattering amplitude data for this target were computed and delivered to APL-UW. The acoustic color computed directly in the xz and xy planes, as well as the reconstruction of the acoustic color in xz plane are shown in Fig. (10). The only geometrical feature that makes this target non-axially symmetric is the semicircular handle. Scattering effects due to this can be seen in Fig. (10b) at frequencies higher than about 20 kHz. Figure (10c) shows the acoustic color in xz plane reconstructed from bistatic scattering amplitude data as was discussed in the previous section.

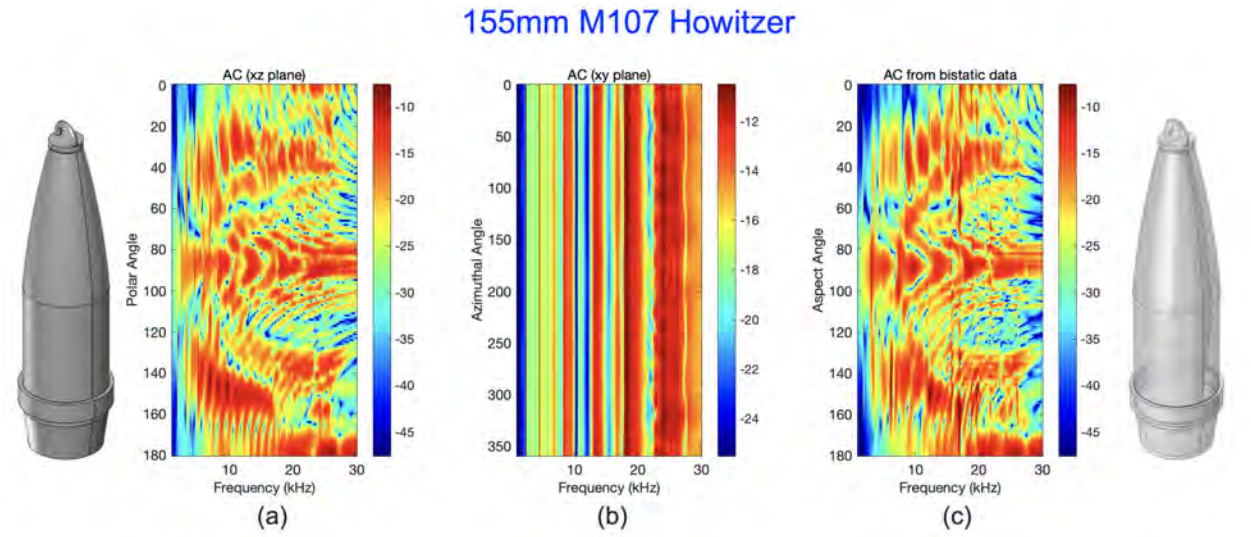

Figure 10: *Panels (a) and (b) show the acoustic color, computed directly, in xz and the xy planes with the target's axis along the z-axis. Panel (c) shows that the acoustic color in the xz plane reconstructed from the bistatic scattering amplitudes computed at points on the surface of a sphere of 10-m radius.*

Results like those in Fig. (9) are shown in Fig. (11)

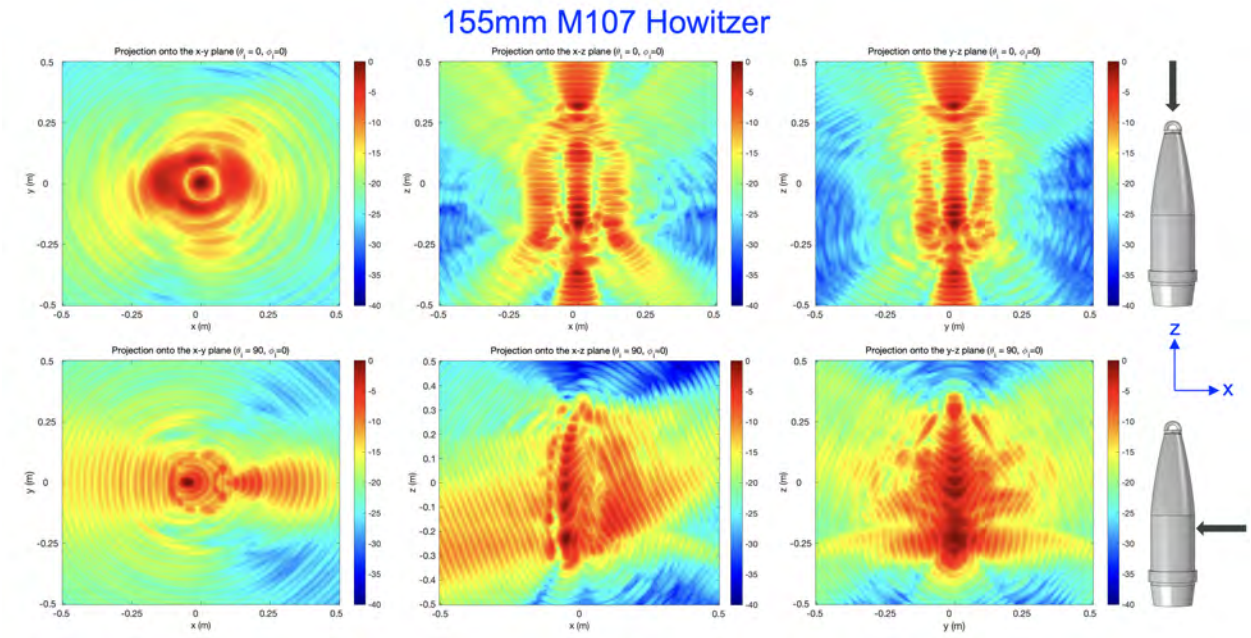

Figure 11: *Projections of the scattered field onto the coordinate surfaces for the 155mm M107 Howitzer. The direction of the incident field is shown in the far right of the figure. Each row shows the results for the indicated incident field and contains the scattered field in the three coordinate planes defined in Fig. (6). The xz plane is the plane of the paper.*

Comparing the middle and the right panels in the top row, we note that the difference is entirely due

to the semicircular handle. While scattering in the middle panel is viewed for the case when the target is in the position shown, the scattering in the right panel is viewed in a plane perpendicular to it. For the rest of the results the same comments apply as those made for Target *c*.

3.3 Target *d*

This target is the 105mm M60. Bistatic scattering amplitudes data for this target have been computed but have not been delivered to APL-UW yet. Results for this target similar to Figs.(7) and (10) are shown in Fig. (12)

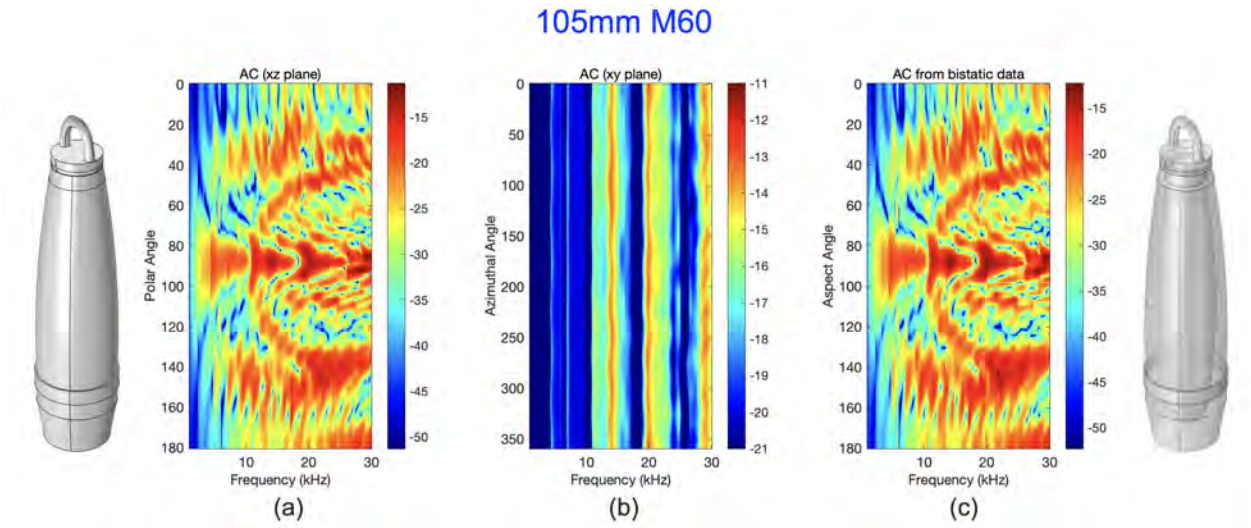

Figure 12: *Panels (a) and (b) show the acoustic color, computed directly, in xz and the xy planes with the target's axis along the z-axis. Panel (c) shows that the acoustic color in the xz plane reconstructed from the bistatic scattering amplitudes computed at points on the surface of a sphere of 10-m radius.*

In addition to the handle, this target has a hole that makes it non-axially symmetric. While the presence of the hole makes the target flooded and drastically changes it scattering characteristics, its contributions cannot be seen in these results unless they are compared with a case when the target is not flooded. The effects of the handle can be seen in Fig. (12b) at higher frequencies, where these effects can be resolved. The reconstructed acoustic color in the xz plane is shown in Fig. (12c), which is almost identical to Fig. (12a).

The projections of the acoustic field onto the coordinate planes for the 105mm M60 are shown in Fig. (13), where the orientation of the target is off by 90° compared to that of the 155mm M107 (Target-*b*). For this reason, the effects of scattering from the handle in the middle panel of the top row of Fig. (13) resembles that of the right panel of the top row in Fig. (11) and vice versa. Furthermore, since the 105mm M60 is flooded, the effects of scattering from its solid parts are much more prominent compared to that of the 155mm M107 Howitzer. This can most clearly be seen in the middle and the right panels of the top row of Fig. (13).

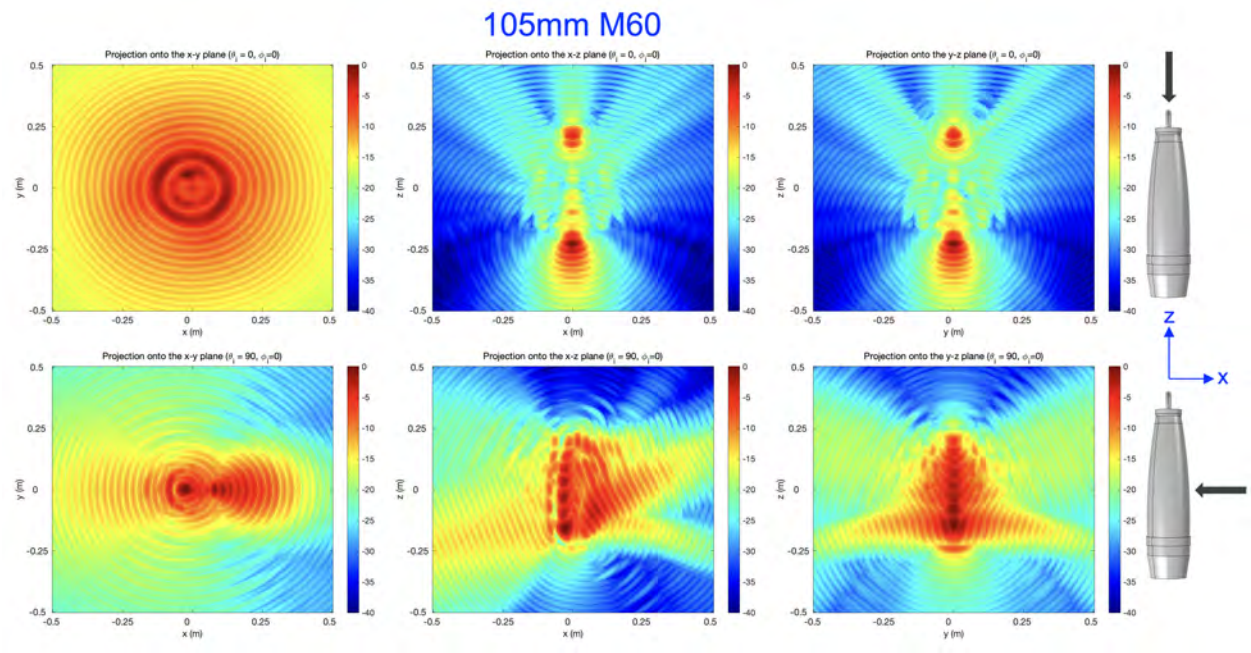

Figure 13: *Projections of the scattered field onto the coordinate surfaces for the 105mm M60. The direction of the incident field is shown in the far right of the figure. Each row shows the results for the indicated incident field and contains the scattered field in the three coordinate planes defined in Fig. (6). The xz plane is the plane of the paper.*

3.4 Target *e*

This target is the 81mm mortar shell. We presented the results for this target in our 2022 Interim Report, but since then the model that we used to compute its bistatic scattering amplitudes has been improved and in this report we presents our updated results. Results similar to those of Fig. (12) for this target are shown in Fig. (14), where the effects scattering from the six fins begin to emerge at frequencies above 15 kHz. The reconstruction of the acoustic color in the xz plane from the bistatic data in Fig. (14c) almost exactly reproduces Fig. (14a).

Projections of the scattered field onto the coordinate surfaces are shown in Fig. (15), where again since the target is flooded, scattering from the walls of the target are more prominent. This can be seen more clearly in the right two panels in the top row. Also, note that these same two panels look almost identical, which is the characteristics of an axially symmetric target. The reason for this is that for an incident field along the axis of the target the fins have very low cross section and thus their contribution to the scattered field is negligibly small. In the middle bottom panel, we see that the incident field, which is perpendicular to the axis of the target, is scattered in two directions by the curved surface of the target. Other observations are similar to those made for the other targets. The bistatic scattering data for this target have also been delivered to APL-UW.

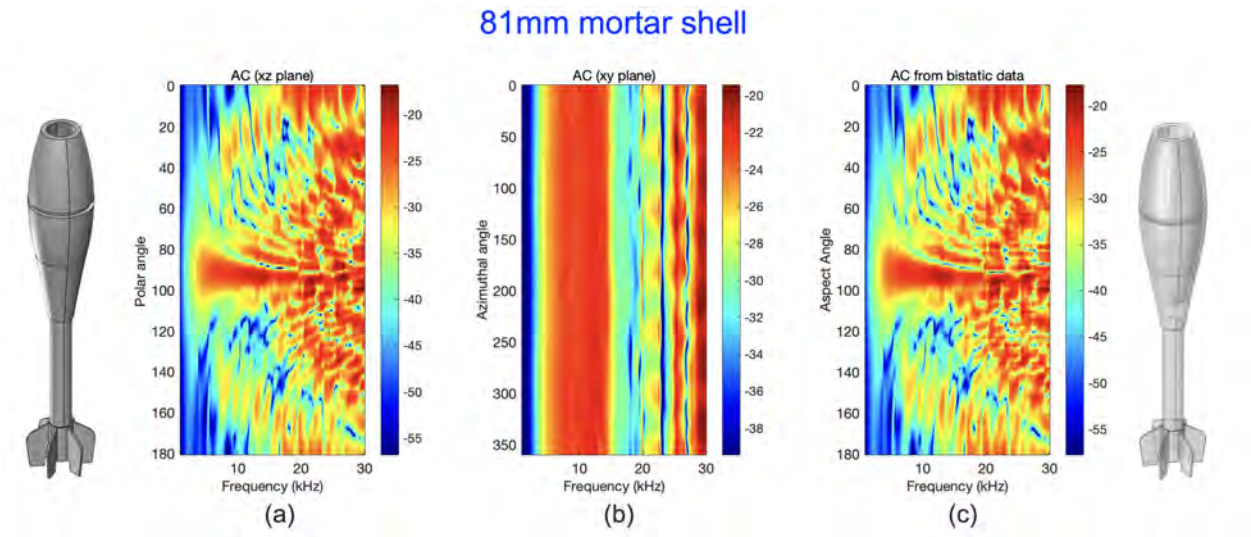

Figure 14: *Panels (a) and (b) show the acoustic color, computed directly, in xz and the xy planes with the target's axis along the z-axis. Panel (c) shows that the acoustic color in the xz plane reconstructed from the bistatic scattering amplitudes computed at points on the surface of a sphere of 10-m radius.*

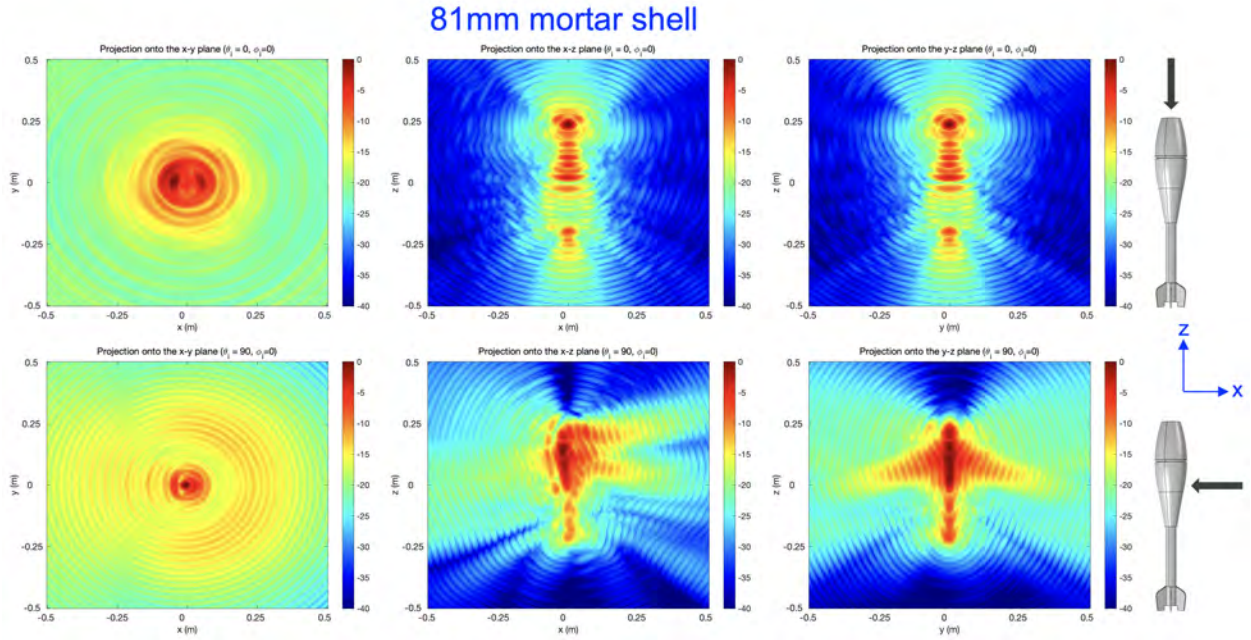

Figure 15: *Projections of the scattered field onto the coordinate surfaces for the 81mm mortar shell. The direction of the incident field is shown in the far right of the figure. Each row shows the results for the indicated incident field and contains the scattered field in the three coordinate planes defined in Fig. (6). The xz plane is the plane of the paper.*

4 Summary and conclusions

During this year, the second of this project, we continued computing bistatic scattering amplitudes on the surface of a sphere of 10-m radius for use in the TIER models. The mathematical justification for the number and the distribution of the points on the surface of the sphere where the bistatic scattering amplitudes are computed was presented in our 2022 Interim Report. In this report we presented results for four targets, where we developed techniques to analyze the generated data, to not only gain physical insight, but also to validate the results. We developed an interpolation technique to reconstruct the acoustic color from the bistatic scattering data computed on the surface of a 10-m sphere and compare the results to the acoustic color computed directly. We showed that this technique can reproduce the acoustic color that looks almost identical to the one computed directly for every target. This exercise not only validates all the parameters that go into computing the data on the surface of the sphere like the number and distribution of the data points, but it also confirms the accuracy and efficacy of the interpolation technique for further use as in the TIER model.

We also developed a method of projection the data from the surface of the sphere onto the coordinate surfaces by back propagation that further enhances our ability to validate the data and gain physical insight into the scattering problem. By application of this technique to every target, we showed that every target possesses a scattering signature that is unique to that target, as expected.

Since the start of the project, we have computed the bistatic scattering amplitudes for five out of the six targets listed in Fig. (4). We are currently working on the sixth target, which is Target f.

During this period, in response to a request from the SERDP Program office, we started working with Dr. David Williams of Penn State to produce scattering data for various targets that can be used to train his classifiers. His data specifications are different from those of APL-UW, and we have made the necessary modifications to our codes to accommodate them. We delivered data for the 81mm Mortar to and an open-ended Howitzer shell to Penn State.

References

[1] A. T. Abawi and P. Krysl, "Coupled finite element/boundary element formulation for scattering from axially-symmetric objects in three dimensions," The Journal of the Acoustical Society of America **142**(6), 3637–3648 (2017).

[2] S. G. Kargl, A. L. España, K. L. Williams, J. L. Kennedy, and J. L. Lopes, "Scattering from objects at a water-sediment interface: Experiment, high-speed and high-fidelity models, and physical insight," IEEE Journal of Oceanic Engineering **40**(3), 632–642 (2015).

[3] Wikipedia, Golden spiral — Wikipedia, The Free Encyclopedia, https://en.wikipedia.org/wiki/Golden_spiral#cite_note-1, 2022, [Online; accessed 22-December-2022].

[4] S. G. Kargl, sERDP Symposium Poster Session, 2022.